Title: Finite Element Modelling of Trabecular Bone Microstructure using Emerging CT Images

Authors: Indranil Guha, Chamith S. Rajapakse, Xiaoliu Zhang, Gregory Chang, Punam K. Saha

Abstract (250 words)

Osteoporosis is a common age-related disease associated with increased bone loss causing reduced bone strength and enhanced fracture-risk. Finite element (FE) modelling is used to estimate bone strength from high-resolution three-dimensional (3-D) imaging modalities including micro-CT, MRI, and HR-pQCT. Emerging technologies of multi-row detector CT (MDCT) imaging offer spatial image resolution comparable to human trabecular thickness. However, at the current MDCT resolution regime, FE modelling based on segmented trabecular bone (Tb) microstructure suffers from noise and other imaging artifacts. In this paper, we present a bone mineral density (BMD)-adjusted FE modeling method of Tb microstructure from MDCT imaging without requiring Tb segmentation. The method spatially varies mechanical stiffness based on local ash-density estimated from MDCT-derived BMD and, thus, models the hypothesis that stress-flow is primarily absorbed by Tb microstructure as compared to marrow space under mechanical compression. Specifically, an MDCT-based linear FE analysis method was developed using a voxel-mesh and the above model of space-varying stiffness, and the performance of the method was examined. For FE analysis, an axial cylindrical image core of 8mm diameter from 4-6% of distal tibia was extracted after aligning the tibial bone axis with the coordinate z-axis of the image space. Intra-class correlation coefficient (ICC) of 0.89 was observed in a repeat MDCT scan reproducibility experiment using cadaveric distal tibia specimens (n = 10). Also, high linear correlation (r = 0.87) was found between von Mises stress values and MDCT based BMD at individual voxels supporting the central hypothesis of our method.

Description of Purpose

Osteoporosis is a common age-related disease characterized by reduced bone mineral density (BMD) leading to diminished bone strength and enhanced fracture-risk. Approximately, 40% of women and 13% of men suffer osteoporotic fractures in their lifetime.[1] Osteoporotic hip fractures reduce life expectancy by 10-20%,[2] and the current upward trend in average life expectancy will increase the expected fracture incidence to 6.3 million by 2050.[3] Dual-energy X-ray absorptiometry (DXA) measured areal BMD is the current clinical standard to define osteoporosis. In general, BMD explains 60-70% of the variability in bone strength and fracture-risk, and the remaining variability is collectively contributed by other factors including cortical and trabecular bone (Tb) distribution, and their microstructural basis.[4]

Finite element (FE) modelling is widely used to computationally estimate bone strength and other mechanical properties.[5-9] Recent technological advances in several three-dimensional (3-D) imaging modalities, including micro-CT imaging, magnetic resonance imaging (MRI),[4,10-12] and high-resolution peripheral quantitative computed tomography (HR-pQCT),[13-15] have enabled *in vivo* acquisition of Tb microstructure and allowed researchers to model computational bone mechanics at microstructural details. Emerging technologies of multi-row detector CT (MDCT) imaging offer *in vivo* spatial image resolution comparable to human trabecular thickness. Also, MDCT imaging offers quantitative BMD at individual voxels and overcomes the major deficits of MRI and HR-pQCT modalities related to slow scan speed, limited field-of-view and failure to provide quantitative BMD.[16] However, at the current MDCT resolution regime, FE analysis (FEA) using segmentation of Tb microstructure and mesh modeling suffers from noise and other imaging artifacts. In this paper, we present an MDCT-based FEA method that does not require segmentation of Tb microstructure. Instead, the method models computational mechanics of Tb microstructure using BMD-adjusted stiffness. Specifically, the FEA method uses ash-density, estimated from MDCT-derived BMD, to define stiffness of individual voxels. In other words, the model simulates an FEA method along the hypothesis that stress-flow is primarily absorbed by Tb microstructure as compared to marrow space under mechanical compression.

Materials and Methods

This section presents a 3-D voxel-based FEA method that models computational mechanics of Tb microstructure using BMD-adjusted stiffness and evaluate its performance. Major modules of materials and methods involved in this project are listed as follows—(1) cadaveric distal tibia specimens, (2) MDCT imaging, (3) BMD-adjusted FE modelling, and (4) experiments and data analysis.

Cadaveric Distal Tibia Specimens

Ten cadaveric ankle specimens were collected under the Deeded Bodies Program, The University of Iowa, Iowa City, Iowa, USA. These specimens were removed at mid-tibia and included the ankle joint and the foot. All soft tissues below the cutting surface were preserved, and the specimens were kept frozen until MDCT imaging.

MDCT Imaging

MDCT imaging was performed on a 128 slice SOMATOM Definition Flash scanner (Siemens, Munich, Germany) at the University of Iowa Comprehensive Lung Imaging Center. Single tube spiral acquisition with the following CT parameters were used to generate high-resolution Tb images—120kV, 200 effective mAs, 1sec rotation speed, pitch factor: 1.0, number of detector rows: 16, scan time: 23.2secs, collimation: 16 × 0.6mm, total effective dose equivalent: 170μSv ≈ 20 days of environmental radiation in the U.S. Siemens z-UHR scan mode was applied, which enables Siemens double z sampling technology allowing a dual sampling of the 0.6mm detectors, splitting the signal so that each detector created a 0.3mm slice in the z plane. After scanning in a helical mode with a 400μm slice thickness, images were reconstructed at 200μm slice-spacing using a normal cone beam method with a special U70u kernel achieving

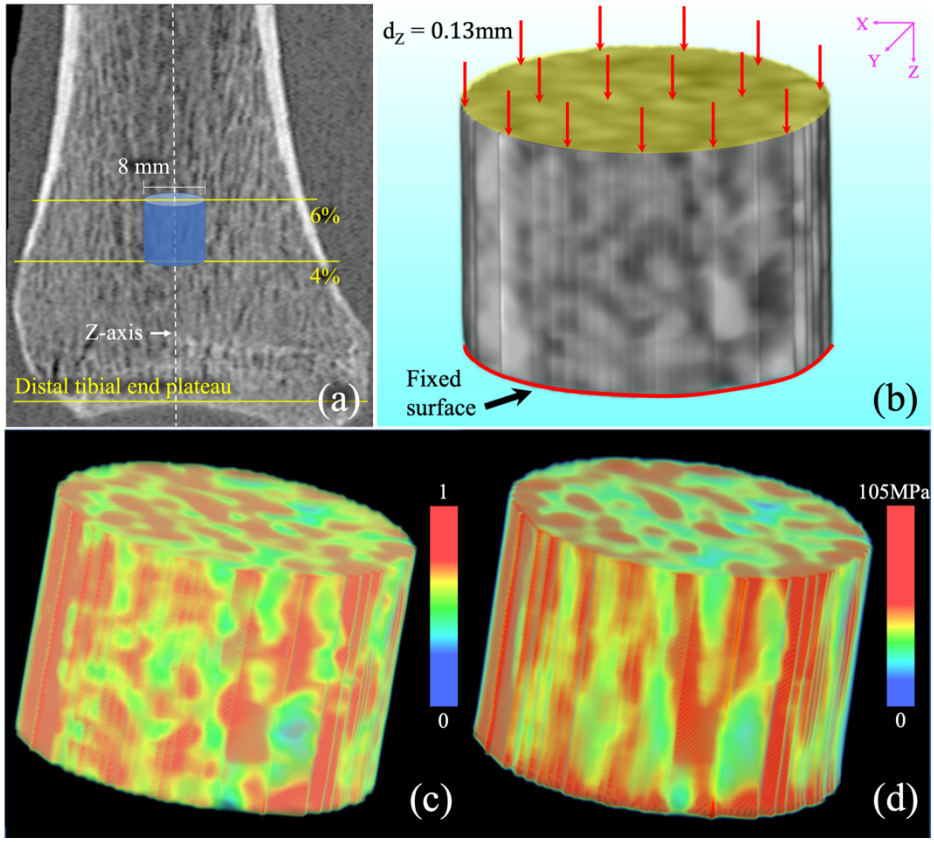

Figure 1. Multi-row detector CT-based FE modelling and computation of trabecular microstructural strength. (a) A sagittal image slice from a distal tibia MDCT scan; the cylindrical ROI for FEA is shown in blue. (b) FEA boundary condition and loading protocol on the extracted Tb core. (c) Color-coded volume rendition of the normalized BMD map over the ROI of (b). (d) Same as (c) but for FEA recorded von Mises stress.

high structural resolution. A Gammex RMI 467 Tissue Characterization Phantom (Gammex RMI, Middleton, WI) was scanned to calibrate CT Hounsfield numbers into BMD (mg/cc) values.

BMD-Adjusted FE Modelling

A compressive FEA method was developed for an upright cylindrical Tb region at an isotropic image resolution. The method was designed and implemented within the computational platform and facilities provided by the ANSYS software (ANSYS Mechanical 2019 R2, Ansys Inc., Southpointe, Pennsylvania, USA). First, the method interpolates the CT-derived BMD image at 150µm isotropic voxels and directly uses the interpolated voxel grid to define the mesh structuring elements. Each voxel is modelled as a cubical element with its center aligned at the voxel coordinate location, and edges are added following the network of the cubical complex representation of a voxel grid.[17] The connectivity within the FE mesh is defined by specifying common vertices and edges between each pair of adjacent voxel or cubical elements. Isotropic mechanical material properties are assigned to each cubic element, where elastic modulus of a cubical element is derived from the BMD value at the corresponding voxel. Let p_e denote the cubical mesh element corresponding to the image voxel p; also, let $\rho_{\mathrm{BMD}}(p)$ denote the BMD value at p derived from MDCT imaging and calibration of CT values using the Gammex phantom and then normalization to the [0 1] scale by dividing with the maximum BMD value over all specimens. The ash density (mg/cc) value at p, denoted by $\rho_{\mathrm{ash}}(p)$, is computed from $\rho_{\mathrm{BMD}}(p)$ using the following equation[9]

$$\rho_{\mathrm{ash}}(p) = 0.0633 + 0.887\rho_{\mathrm{BMD}}(p), \text{ where } 0 \le \rho_{\mathrm{BMD}}(p) \le 1. \quad (1)$$

The elastic modulus (unit: MPa) of the cubical mesh element p_e corresponding to the image voxel p, denoted by $E(p_e)$, is derived from $\rho_{\mathrm{ash}}(p)$ following the equation by Keyak *et al.*[18]

$$E(p_e) = 21700 \cdot \rho_{\mathrm{ash}}^{2.07}(p). \quad (2)$$

Finally, a Poisson's ratio of 0.3 is assigned to all elements.[8] Boundary conditions are imposed to simulate a physical mechanical experiment of axial compressive loading. Specifically, the bottom surface of the cylindrical region of interest (ROI) is fixed in all three coordinate directions, and a constant displacement along the coordinate z-direction is applied on all vertices at the top surface while restricting their movements along the x- and y-directions.

Experiments and Data Analysis

Cadaveric ankle experiments were executed to evaluate the repeat scan reproducibility and to examine the relationships between stress and BMD. To examine the reproducibility, three repeat scans were acquired for each cadaveric specimen after repositioning the specimen on the CT table before each scan. Each cadaveric ankle CT scan was paired with a Gammex phantom scan, which was used

to calibrate CT Hounsfield numbers into BMD values. BMD images were interpolated at 150µm isotropic voxel size using a windowed sync interpolation method. The tibial bone region was segmented from the BMD image using connectivity analysis and morphological operations, and the tibial bone axis was computed.[19] The BMD image was transformed to align the tibial bone axis with the coordinate z-axis so that the longitudinal trabeculae are predominantly upright.

These upright BMD images at 150µm isotropic voxels were used for FEA. An upright cylindrical ROI of diameter 8mm covering 4-6% of distal tibial site along the z-direction was harvested from each upright BMD image (see Figure 1(a)); an average tibial length of 34cm was used to define the 4-6% of tibial site. The 3-D 8-Node structural solid (SOLID185) within the ANSYS software was selected to represent cubic mesh elements, and a linear equation solver was applied with an automatic time-stepping option. The boundary conditions were imposed as described earlier and a total displacement of 0.13mm (~2% of the ROI length) (see Figure 1(b)) was applied on the BMD-adjusted FE mesh model over 10 iterations. Young's modulus was computed using applied strain and the average von Mises stress (unit: MPa)[20] of elements on the top surface.

BMD calibration, upright bone alignment, ROI selection, and FEA steps were independently applied on repeat CT scans to determine reproducibility of the combined process including CT imaging as well as the comprehensive analytic protocol. Intra-class correlation coefficient (ICC) of computed modulus values from repeat CT scan was calculated to examine the reproducibility of the method. To determine the relationship between BMD and stress, linear correlation between BMD values and observed von Mises stresses at individual voxels on the middle axial slice of all ten specimens was computed; the image and FEA data of the first scans of each specimen was used for this analysis.

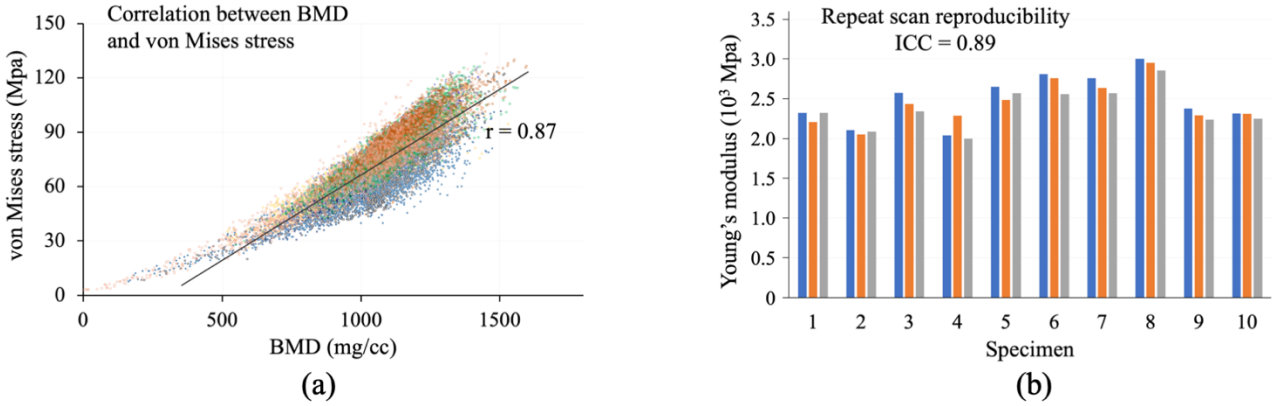

Figure 2. Quantitative evaluation of multi-row detector CT (MDCT)-based FE modelling. (a) Linear correlation (r value) between computed von Mises stress and BMD at individual voxels on axial slices at the middle of the specimen along its length. (b) Repeat scan reproducibility of MDCT-based FE analysis. Computed Young's modulus from three repeat scans of each specimen are shown.

Results

The new BMD-adjusted FEA method was successfully applied on three repeat scans of all ten cadaveric specimens used in our experiments. The method was run on a Linux machine equipped with octa-core Xeon Gold 3.60GHz CPUs with 64GB of RAM and required an average computation time of 40 minutes per MDCT scan. Figure 1 presents qualitative results of FEA over a cylindrical Tb ROI. Figure 1(a) and (b) illustrate the ROI selection and FEA application processes. Color-coded illustrations of normalized BMD map and FEA based von Mises stress over the target Tb ROI are shown in (c) and (d), respectively. Visual correspondence between Tb microstructures (red) in (c) and high stress lines (red) in (d) may be noted, which supports the central hypothesis that stress primarily propagates through Tb voxels with high stiffness compared to the marrow voxels with low stiffness. Results of quantitative analysis evaluating the performance of our MDCT-based FE modelling are presented in Figure 2. A high linear correlation (r = 0.87) was observed between computed von Mises stress and BMD at individual voxels, which further validates the qualitative observations of Figure 1 and the principle of our BMD-based FEA. Also, a high repeat MDCT scan reproducibility (ICC = 0.89) of FEA-derived Young's modulus was observed. Both qualitative and quantitative experimental results suggest that the comprehensive protocol of MDCT-based FEA of quantitative Tb microstructural strength as presented in this paper is effective and reproducible.

Conclusions

An emerging MDCT-based method is presented to compute the strength of Tb microstructure using a new BMD-adjusted FE modelling and analytic method. Experimental results have shown that our BMD-adjusted FEA method of computing Tb microstructural strength is reproducible and support the central hypothesis that computational stresses follow Tb microstructure fuzzily characterized by high BMD values at the current regime of *in vivo* CT resolution.

New or breakthrough work to be presented

1) An emerging MDCT-based method for computing trabecular bone microstructural strength that is applicable *in vivo*
2) A BMD-adjusted FE modeling and analytic protocol on image voxel grid

3) Evaluation of the relationship between computational stress and bone mineral density fuzzily characterizing trabecular bone micro-network

4) Evaluation of repeat scan reproducibility of the new MDCT-based method of computing trabecular bone microstructural strength

Publication status: This work has NOT been submitted for publication or presentation elsewhere.

Acknowledgements: This work was supported by the NIH grant R01 HL142042.

References

[1] TWHO Bulletin, "Aging and Osteoporosis," 1999.

[2] LJ Melton, 3rd, "Epidemiology of fractures," in *Osteoporosis: Etiology, Diagnosis, and Management*, B. L. Riggs and L. J. Melton, 3rd, Eds., New York, Raven Press, 1988, pp. 133-154.

[3] C Cooper, G Campion, and LJ Melton, 3rd, "Hip fractures in the elderly: a world-wide projection," *Osteoporosis International*, **2**, 285-289, 1992.

[4] FW Wehrli, PK Saha, BR Gomberg, HK Song, PJ Snyder, M Benito, A Wright, and R Weening, "Role of magnetic resonance for assessing structure and function of trabecular bone," *Topics in Magnetic Resonance Imaging* **13**, 335-355, 2002.

[5] G Chang, CS Rajapakse, C Chen, A Welbeck, K Egol, RR Regatte, PK Saha, and S Honig, "3-T MR Imaging of proximal femur microarchitecture in subjects with and without fragility fracture and nonosteoporotic proximal femur bone mineral density," *Radiology*, **287**, 608-619, 2018.

[6] A Hotca, CS Rajapakse, C Cheng, S Honig, K Egol, RR Regatte, PK Saha, and G Chang, "In vivo measurement reproducibility of femoral neck microarchitectural parameters derived from 3T MR images," *Journal of Magnetic Resonance Imaging*, **42**, 1339-1345, 2015.

[7] CS Rajapakse, JF Magland, MJ Wald, XS Liu, XH Zhang, XE Guo, and FW Wehrli, "Computational biomechanics of the distal tibia from high-resolution MR and micro-CT images," *Bone*, **47**, 556-563, 2010.

[8] N Zhang, JF Magland, CS Rajapakse, YA Bhagat, and FW Wehrli, "Potential of in vivo MRI-based nonlinear finite-element analysis for the assessment of trabecular bone post-yield properties," *Medical Physics*, **40**, 1-10, 2013.

[9] J Keyak, S Sigurdsson, G Karlsdottir, D Oskarsdottir, A Sigmarsdottir, J Kornak, T Harris, G Sigurdsson, B Jonsson, and K Siggeirsdottir, "Effect of finite element model loading condition on fracture risk assessment in men and women: the AGES-Reykjavik study," *Bone*, **57**, 18-29, 2013.

[10] S Majumdar, D Newitt, A Mathur, D Osman, A Gies, E Chiu, J Lotz, J Kinney, and H Genant, "Magnetic resonance imaging of trabecular bone structure in the distal radius: relationship with X-ray tomographic microscopy and biomechanics," *Osteoporos International*, **6**, 376-385, 1996.

[11] TM Link, S Majumdar, P Augat, JC Lin, D Newitt, Y Lu, NE Lane, and HK Genant, "In vivo high resolution MRI of the calcaneus: differences in trabecular structure in osteoporosis patients," *Journal of Bone and Mineral Research*, **13**, 1175-1182, 1998.

[12] G Chang, SK Pakin, ME Schweitzer, PK Saha, and RR Regatte, "Adaptations in trabecular bone microarchitecture in Olympic athletes determined by 7T MRI," *Journal of Magnetic Resonance in Medicine* **27**, 1089-1095, 2008, PubMed Central PMCID: PMCPMC3850284.

[13] S Boutroy, ML Bouxsein, F Munoz, and PD Delmas, "*In vivo* assessment of trabecular bone microarchitecture by high-resolution peripheral quantitative computed tomography," *The Journal of Clinical Endocrinology and Metabolism*, **90**, 6508-6515, 2005.

[14] M Burrows, D Liu, and H McKay, "High-resolution peripheral QCT imaging of bone micro-structure in adolescents," *Osteoporosis International*, **21**, 515-520, 2010.

[15] R Krug, AJ Burghardt, S Majumdar, and TM Link, "High-resolution imaging techniques for the assessment of osteoporosis," *Radiologic Clinics of North America*, **48**, 601-621, 2010, PubMed Central PMCID: PMC2901255.

[16] TM Link, "Osteoporosis imaging: state of the art and advanced imaging," *Radiology*, **263**, 3-17, 2012, PubMed Central PMCID: PMC3309802.

[17] PK Saha, R Strand, and G Borgefors, "Digital topology and geometry in medical imaging: a survey," *IEEE Transactions on Medical Imaging*, **34**, 1940-1964, 2015.

[18] J Keyak, I Lee, D Nath, and H Skinner, "Postfailure compressive behavior of tibial trabecular bone in three anatomic directions," *Journal of Biomedical Materials Research*, **31**, 373-378, 1996.

[19] C Chen, X Zhang, J Guo, D Jin, EM Letuchy, TL Burns, SM Levy, EA Hoffman, and PK Saha, "Quantitative imaging of peripheral trabecular bone microarchitecture using MDCT," *Medical Physics*, **45**, 236-249, 2018.

[20] DL Logan, *A first course in the finite element method*, Cengage Learning, 2011.